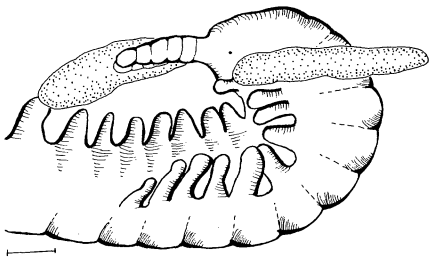

Fig. 3. Illustration of the lateral view of the left side of the fossil onychophoran shown in Fig. 2 (bar = 0.5 mm).

defense. An association of *A. pedunculata* with sponges has been suggested (*3*), but it is not clear whether *Aysheaia* actually fed on the sponges or scraped material such as algae deposits off the surface of sponges. Early terrestrial forms might have fed on decaying plant and animal matter. Plant remains do occur in the alimentary tract of extant velvet worms (*11*). At one point in their terrestrial evolution, onychophorans developed predatory habits, at which time the production of slime was used to capture prey.

Velvet worms have always presented an enigma because it was thought that they were not robust enough to survive rafting or transport (*12, 13*), and the eggs of oviparous forms are not durable (*14*). Yet, today velvet worms occur on several islands of the Greater Antilles, including Hispaniola (*13*). There are two basic schools of thought regarding the appearance of animals on the Greater Antilles: dispersion and vicariance. There is no plausible explanation of velvet worm distribution with the dispersal hypothesis, thus it appears that the present distribution supports the vicariance hypothesis: namely, that the velvet worms already formed a portion of the biota that occupied the ancient "proto-Antillean Archipelago" before it moved into its present position as the Greater Antilles (*15, 16*).

The present distribution of velvet worms is predominately gondwanan (*13*). Two hypotheses have been proposed to explain this phenomenon (*17*). The first is that the invasion of land by these creatures occurred in the Southern Hemisphere, whereas the alternative suggests that terrestrial invasion was universal but the environment of the Laurasian land masses somehow became unsuitable for the continued existence of velvet worms. The presence of a fossil velvet worm in Baltic amber provides evidence that these animals existed in northern Europe in the Eocene and indicates that their range was more extensive in the past, possibly even pantropical and pansubtropical.

REFERENCES AND NOTES

1. V. Storch and H. Ruhberg, in *Microscopic Anatomy of Invertebrates*, F. W. Harrison and E. M. Rice, Eds. (Wiley-Liss, New York, 1993), pp. 11–56.
2. S. M. Manton, *The Arthropoda: Habits, Functional Morphology and Evolution* (Clarendon, Oxford, 1977).
3. H. B. Whittington, *Philos. Trans. R. Soc. London Ser. B* **284**, 165 (1978).
4. R. A. Robison, *J. Paleontol.* **59**, 226 (1985).
5. J. Dzik and G. Krumbiegel, *Lethaia* **22**, 169 (1989).
6. I. Thompson and D. S. Jones, *J. Paleontol.* **54**, 588 (1980).
7. S. J. Gould, *Wonderful Life* (Norton, New York, 1989).
8. G. O. Poinar Jr., *Life in Amber* (Stanford Univ. Press, Stanford, CA, 1992).
9. D. R. Nelson, in *Ecology and Classification of North American Freshwater Invertebrates*, J. H. Thorp and A. P. Covich, Eds. (Academic Press, San Diego, CA, 1991), pp. 501–521.
10. A. M. Simonetta and L. Delle Cave, *Acad. Naz. Lincei Roma* **49**, 389 (1981).
11. E. L. Bouvier, *Ann. Sci. Nat. (Zool.)* **2**, 1 (1905).
12. P. J. Darlington Jr., *Biogeography of the Southern End of the World* (Harvard Univ. Press, Cambridge, MA, 1965).
13. C. T. Brues, *Am. Nat.* **57**, 210 (1923).
14. Many species in both of the present-day families of velvet worms, that is, the Peripatidae and the Peripatopsidae, are viviparous (*1*).
15. D. E. Rosen, *Syst. Zool.* **24**, 431 (1976).
16. The proto-Antillian Archipelago was formed sometime in the Mesozoic between North and South America. Through the forces of plate tectonics, this land mass moved eastward into what is now the Caribbean Sea and broke up into the various island groups known as the Greater Antilles (*15*).
17. N. N. Tait, D. A. Briscoe, D. M. Rowell, *Mem. Assoc. Australas. Palaeontol.* **18**, 21 (1995).

18. I thank A. Boucot, N. Tait, and R. Poinar for comments and J. Santiago-Blay for assistance with obtaining literature on velvet worms. The specimens are deposited in the Poinar Amber Collection maintained at Oregon State University.

24 May 1996; accepted 10 July 1996

Threefold Electron Scattering on Graphite Observed with C_{60}-Adsorbed STM Tips

K. F. Kelly, D. Sarkar, G. D. Hale, S. J. Oldenburg, N. J. Halas*

The scanning tunneling microscope (STM) has been used to observe threefold symmetric electron scattering from point defects on a graphite surface. These theoretically predicted electronic perturbations could not be observed with a bare metal tip but could only be imaged when a fullerene (C_{60}) molecule was adsorbed onto the tunneling region (apex) of an STM tip. Functionalizing an STM tip with an appropriate molecular adsorbate alters the density of states near the Fermi level of the tip and changes its imaging characteristics.

The STM has recently enabled scientists to image local surface electronic phenomena on the nanometer scale. On metal surfaces, the STM has been used to image scattering of surface-state electrons around point defects and electron interference within and around "quantum corrals" (*1*). We report the observation of a threefold symmetric electron scattering process around point defects on graphite. These electron scattering patterns are in almost exact agreement with the theoretical predictions of this phenomenon by Mizes and Foster (*2*). The patterns were observable only when an STM tip had a C_{60} molecule adsorbed onto its tunneling region. This result shows that molecular functionalization that controls the local density of states of an STM tip can permit the observation of an electronic effect not observable with a bare metal STM tip.

The functionalization of STM tips with C_{60} to control the electronic interactions between the tip and surface is similar to the attachment of molecules to atomic force microscope tips to control the chemical forces between the tip and surface (*3*). However, instead of exhibiting a sensitivity to chemical forces, the tunneling current of the STM is sensitive to the local density of states at the Fermi energy (E_F) of both the surface and the tip. The adsorption of a molecule such as C_{60} onto an STM tip, which can act as a tunneling site, alters the local density of states of the tip in the vicinity of E_F, thereby modifying the tunneling current and changing the way the tip samples the electronic states of the surface it is imaging.

Resh *et al.* have reported improved atomic resolution on graphite when fullerenes were adsorbed onto STM tips (*4*). We have also reported the in situ characterization of C_{60} adsorbed onto the active region of tunneling tips by "inverse imaging" (*5*). Inverse imaging of the C_{60}-adsorbed STM tips enables one to determine the number of fullerenes in the tunneling region and also shows that the adsorbed fullerene molecule or molecules can function as a tunneling site or sites. Inverse imaging is a robust and highly reproducible method for monitoring the structure of an STM tip at the tunneling junction (*6*).

To create the fullerene-adsorbed STM tips, we vacuum-deposited a thin fullerene film (100 to 500 Å) onto highly oriented

Department of Electrical and Computer Engineering, Rice Quantum Institute, and Center for Nanoscale Science and Technology, Rice University, Post Office Box 1892, Houston, TX 77251, USA.

*To whom correspondence should be addressed.

pyrolytic graphite (HOPG). The C_{60} molecules of the film are weakly bound to each other and to the graphite substrate (*7*). A cut Pt-Rh (87:13) STM tip is then lowered into the film and rastered through the film (*4*). The C_{60} molecules preferentially adsorb onto the Pt tip, undergoing charge transfer from the metal to the adsorbate (*8*). This C_{60}-metal interaction is strong enough to prevent the C_{60} from diffusing along the metal surface and from rotating in place, as has been observed in the bulk solid at room temperature (*8*, *9*). Thus, the C_{60} adsorbate can create a relatively stable tunneling site on the apex of the STM tip. By analogy with tunneling sites on metallic tips, multiple C_{60} molecules adsorbed onto the tunneling junction produced images with poor atomic resolution, whereas tips with a single or a single predominant C_{60} molecule produced images of graphite with high-quality atomic resolution.

Defects on a graphite surface were created by low-energy Ar^+ bombardment of freshly cleaved HOPG. The incident ion energies ranged from 40 to 65 eV at a fluence of $\sim 10^{11}$ ions per square centimeter. Defects on graphite produced by this procedure have been studied by several groups (*10*, *11*). We imaged the ion-damaged surfaces with a bare Pt-Rh tip to confirm that the defect morphology and density relative to the incident ion dosage agreed with earlier experiments. Subsequent imaging of the graphite defects with C_{60}-adsorbed STM tips revealed inverse images of C_{60} and images of threefold symmetric electron scattering.

Two experimental images of defects on graphite acquired with a C_{60}-adsorbed STM tip are shown in Fig. 1, A and B. These images display the "arms" of the threefold scattering pattern, as well as a $\sqrt{3} \times \sqrt{3}$ electronic scattering modulation termed a "superlattice" in the immediate vicinity of each defect. The threefold symmetry arises because the electrons of the two-dimensional hexagonal lattice layers of graphite scatter about each defect along the three crystallographic directions. The structure of each accompanying superlattice modulation depends on the specific morphology of the central defect (*2*). If an appropriately prepared C_{60} adsorbed tip is used, these electron scattering patterns are imaged easily, reproducibly, and frequently. Figure 1, C and D, show two of the theoretical images of the electrons at E_F directly surrounding point defects in graphite (*2*). Both are "multiple point defects," that is, defects due to two contiguous adsorbate atoms positioned directly on the atomic sites of the graphite lattice and differing from each other only in the orientation of the pair of defects relative to the graphite lattice. The agreement of the scattering arms and the shapes of the superlattice modulations between the observed and the calculated defects is excellent.

Different modulations have been observed in the vicinity of some defects on graphite with bare metal tips (*10*, *12*, *13*). In fact, attempts to explain why threefold electron scattering patterns were not observed led to revised theories for electron scattering on graphite surfaces (*13*). In the course of this study, these other modulations were imaged with metal tips near some defects on the ion-damaged graphite surfaces. However, in no case did we observe the distinct threefold electron scattering patterns when defect-covered graphite surfaces were scanned with a bare metal tip. In fact, on the occasions when the C_{60} molecule desorbed or diffused from the tunneling junction during scanning, the threefold electron scattering patterns abruptly disappeared, yet the arrangement of the defects on the surface remained the same, indicating a highly localized change of the tip apex.

Imaging of graphite defects with C_{60} adsorbed onto the STM tip resulted in either images of threefold symmetric electron scattering or inverse images of the C_{60}-adsorbed tip (*14*). These observations can be explained by the theory of Mizes and Foster (*2*). Both types of images are due to the presence of either single- or multiple-point defects, but the observed STM images depend on the location and orientation of the defects relative to the underlying graphite lattice. The atoms of the graphite surface layer reside in two inequivalent sites: the A-site atom is located directly above an atom of the second layer, and the B-site atom is located directly above a hollow site of the second layer. This inequivalence shifts the energies of the A-site atoms away from the E_F, so the STM images only the B-site atoms of the graphite lattice at low bias voltages (*15*). Therefore, electron scattering around a defect situated on a B-site atom should be easily observable in an STM image, but electron scattering around a defect situated on an A-site atom should not be observable in an STM image. Although the A-site defect does not give rise to an electron scattering pattern, it both perturbs the electronic states of the surrounding atoms and protrudes slightly from the surface plane, thus serving to produce the "inverse image" of the C_{60} adsorbate on the STM tip (*5*, *16*).

The strong chemisorption of fullerenes to most metals shifts the lowest unoccupied molecular orbital (LUMO) of the C_{60} close to the E_F of the metal tip upon adsorption (*17*) and creates a partially filled molecular level at the apex of the tunneling tip near E_F. This molecular adsorbate level, which is narrow in energy compared to the bulk bands of the tip, may enable the C_{60}-adsorbed tip to resolve the electron scattering at E_F of graphite when bare metallic tips cannot. Because the LUMO level of the fullerene is only partially filled, the threefold images are observable symmetrically at both positive and negative low-bias voltages ($-0.5 < V < +0.5$). The total tunneling current is more than the sum of the tunneling electrons at each energy level; it depends on a convolution of the occupied

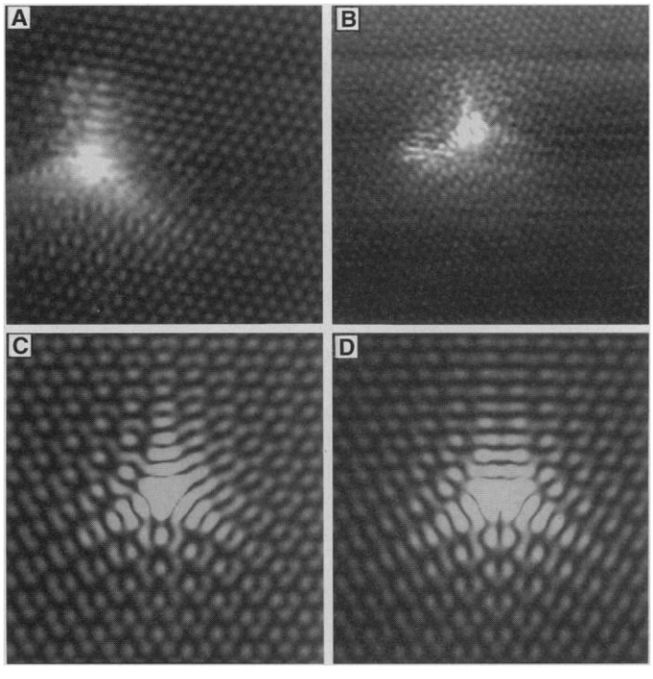

Fig. 1. (**A** and **B**) Constant-current images of defects on graphite observed with a C_{60} molecule attached to the apex of the STM tip (*18*). Tunneling parameters were as follows: (A) 1 nA and 100-mV tip bias, 56 Å by 56 Å by 2.6 Å; (B) 1 nA and −100-mV tip bias, 92 Å by 92 Å by 4.5 Å. (**C** and **D**) Two of the theoretically predicted images of point defects on graphite generated by Mizes and Foster (*2*).

and unoccupied states with the wave-function overlap of the tip and sample. A narrow local density of states at the tip may also explain why these electron scattering patterns could be imaged in a topographic, rather than spectroscopic, mode.

REFERENCES AND NOTES

1. M. F. Crommie, C. P. Lutz, D. M. Eigler, *Nature* **363**, 524 (1993); Y. Hasegawa and P. Avouris, *Phys. Rev. Lett.* **71**, 1071 (1993); M. F. Crommie, C. P. Lutz, D. M. Eigler, *Science* **262**, 218 (1993).
2. H. A. Mizes and J. S. Foster, *Science* **244**, 559 (1989).
3. C. D. Frisbie, L. F. Rozsnyai, A. Noy, M. S. Wrighton, C. M. Lieber, *ibid.* **265**, 2071 (1994).
4. J. Resh *et al.*, *Surf. Sci.* **316**, L1601 (1994).
5. K. F. Kelly *et al.*, *J. Vac. Sci. Technol. B* **14**, 593 (1996).
6. S. Heike, T. Hashizume, Y. Wada, *ibid.*, p. 1522. We have also imaged *tert*-butyl mercaptan molecules bonded to gold STM tips (K. F. Kelly, unpublished data).
7. C. Girard, P. Lambin, A. Dereux, A. A. Lucas, *Phys. Rev. B* **49**, 11425 (1994).
8. H. P. Lang *et al.*, *Europhys. Lett.* **18**, 29 (1992).
9. T. Chen *et al.*, *J. Vac. Sci. Technol. B* **10**, 170 (1992).
10. G. M. Shedd and P. E. Russell, *J. Vac. Sci. Technol. A* **9**, 1261 (1991).
11. H. Kang *et al.*, *Nucl. Instrum. Methods Phys. Res. B* **67**, 312 (1992); D. Marton *et al.*, *Surf. Sci.* **326**, L489 (1995).
12. J. P. Rabe, M. Sano, D. Batchelder, A. A. Kalatchev, *J. Microsc.* **152**, 573 (1988); J. Xhie, K. Sattler, U. Muller, N. Venkateswaran, G. Raina, *Phys. Rev. B* **43**, 8917 (1991).
13. G. M. Shedd and P. E. Russell, *Surf. Sci.* **266**, 259 (1992); J. Valenzuela-Benavides and L. Morales de la Garza, *ibid.* **330**, 227 (1995).
14. Another type of defect formed by low-energy ion bombardment is a subsurface defect in which an ion is trapped between the first and second layers of the graphite without disrupting the lattice. Images of subsurface defects appear essentially the same when imaged with either bare metal or C_{60}-adsorbed tips.
15. D. Tománek *et al.*, *Phys. Rev. B* **35**, 7790 (1987); S. Gwo and C. K. Shih, *ibid.* **47**, 13059 (1993).
16. An adsorbate located in a hollow site on graphite would not give rise to an electron scattering pattern because the scattered waves emanating from each nearest B-site atom would differ in phase by $2\pi/3$ and would sum to zero (*2*).
17. T. R. Ohno *et al.*, *Phys. Rev. B* **44**, 13747 (1991).
18. In filtering all experimental images we used a low-pass filter and all images were acquired in an ambient atmosphere.

19. We thank P. Nordlander and H. Rohrer for helpful discussions on the imaging mechanism, J. W. Rabalais for valuable input on generating defects on graphite, and H. A. Mizes for insightful comments and for providing the figures from his original paper (*2*). Supported by the National Science Foundation (NSF), the Texas Advanced Technology Program, and the Robert A. Welch Foundation. N.J.H. is a recipient of an NSF Young Investigator Award.

1 April 1996; accepted 17 July 1996

Antagonistic Interactions Between Wingless and Decapentaplegic Responsible for Dorsal-Ventral Pattern in the *Drosophila* Leg

William J. Brook and Stephen M. Cohen*

Subdivision of the limb primordia of *Drosophila* into anterior and posterior compartments triggers cell interactions that pattern the legs and wings. A comparable compartment-based mechanism is used to pattern the dorsal-ventral axis of the wing. Evidence is presented here for a mechanism based on cell interaction, rather than on compartment formation, that distinguishes dorsal from ventral in the leg. Mutual repression by Wingless and Decapentaplegic signaling systems generates a stable regulatory circuit by which each gene maintains its own expression in a spatially restricted domain. Compartment-independent patterning mechanisms may be used by other organisms during development.

Short-range interactions between cells in adjacent compartments control growth and patterning in developing limbs [reviewed in (*1*)]. The secreted protein Hedgehog (HH) is expressed by cells of the posterior compartment of the wing imaginal disc and induces expression of another secreted signaling molecule Decapentaplegic (DPP) in nearby anterior cells (*2–5*). DPP serves as a long-range signal that relays information from the anterior-posterior (A-P) interaction to pattern the wing in a symmetric manner (*4–8*). A similar signal-relay system is used in the leg disc, but the situation is complicated by the fact that HH induces DPP expression in dorsal anterior cells while Wingless (WG) and lower levels of DPP are induced in ventral anterior cells (*2*, *9*) (Fig. 1, A and B). The different interpretation of the HH signal in dorsal and ventral leg regions reflects an underlying subdivision of the leg disc into dorsal and ventral quadrants, in which DPP and WG play central roles in patterning the leg (*1*, *10*). The distinction between dorsal and ventral fates in the leg is made differently from that in the developing wing. Expression of the selector gene *apterous* specifies the dorsal compartment of the wing (*11*, *12*). Evidence for a comparable subdivision of the leg into dorsal and ventral lineage compartments is not compelling (*13*), raising the question of whether this distinction depends on a selector gene.

WG activity specifies ventral cell fate in the leg. In larvae mutant for *wg* or for genes in the WG signal transduction pathway, ventral structures are lost and are replaced by a symmetric duplication of dorsal structures (*10*, *14–18*). Furthermore, ectopic expression of WG or activation of the WG signal transduction pathway in cells on the dorsal side of the leg respecifies dorsal cells to ventral fate and causes dorsal-ventral (D-V) axis duplication (*9*, *19–22*). WG is expressed in a wedge of anterior cells adjacent to the A-P compartment boundary on the ventral side of the leg imaginal disc (Fig. 1A) (*14*, *16*). *dpp* is expressed in a stripe of anterior cells adjacent to the A-P boundary, but at higher levels in dorsal cells, which do not express WG (Fig. 1B) (*23*, *24*). We found that the pattern of *dpp* expression is altered in wg^{cx3}/wg^{cx3} leg discs, which have reduced WG activity (*25*) (Fig. 1D). Expression of a *dpp-lacZ* reporter gene is increased on the ventral side, resulting in a symmetric pattern of expression at a level equivalent to that on the dorsal side. Consistent with this pattern of DPP expression, larvae homozygous for the wg^{cx3} mutation develop legs that have dorsal-dorsal symmetry (*10*, *14*). These results suggest that one function of WG in specifying ventral cell fate is to reduce the levels of *dpp* expression in ventral cells.

DPP activity is required to specify dorsal cell fate in the leg. In weak *dpp* mutants, dorsal structures are replaced by symmetrically duplicated ventral structures (*10*). We found that reducing DPP activity in dpp^{d6}/dpp^{d12} leg discs (*26*) alters the pattern of WG expression from its normal ventral domain into an expanded domain along the dorsal A-P boundary (Fig. 1, A and C) (*27*). The domain of ectopic WG expression corresponds to the region of the disc that is transformed to ventral fate in this mutant (*10*). Thus, one function of DPP is to repress WG expression in dorsal cells. This suggestion is supported by the recent observation that clones of cells mutant for *Mad*, a component of the DPP signal transduction pathway, express WG when such clones are located on the dorsal side of the antennal disc near the A-P compartment boundary (*28*).

Taken together, these results suggest that an important aspect of D-V fate specification involves mutual repression by the WG and DPP signaling systems. To further test this model, we asked whether ectopic expression

European Molecular Biology Laboratory, Meyerhofstr 1, 69117 Heidelberg, Germany.

*To whom correspondence should be addressed. E-mail: scohen@embl-heidelberg.de